Chapter 5

Time-Domain Backup Protection for Converter Dominated Hybrid AC-DC Microgrids

Integrating microgrids with renewable energy sources to the national grid has several advantages. With the increase in inherent DC sources, such as solar power plants, and DC electric loads, like electric vehicles, data centers, and household gadgets, the demand for hybrid AC-DC microgrid is enhanced [21]. The connection of AC and DC power sources and loads at their respective subgrid reduces the number of conversion stages and increases overall system efficiency and reliability[21]. A hybrid microgrid finds applications for power quality improvement and voltage profile improvement of the AC microgrid [21]. Increasing the number of electric vehicles on the road also leads to the enhanced demand for DC subgrids for providing the charging facility to electric vehicles [23]. On the other hand, the interconnection of AC and DC subgrids increases the overall operational complexity of the hybrid microgrid. Protection schemes designed solely for AC or DC system may not adequately address all potential fault scenarios in hybrid microgrids. Thus, there is a scope for the development of backup protection for hybrid microgrid using measurements at the PCC.

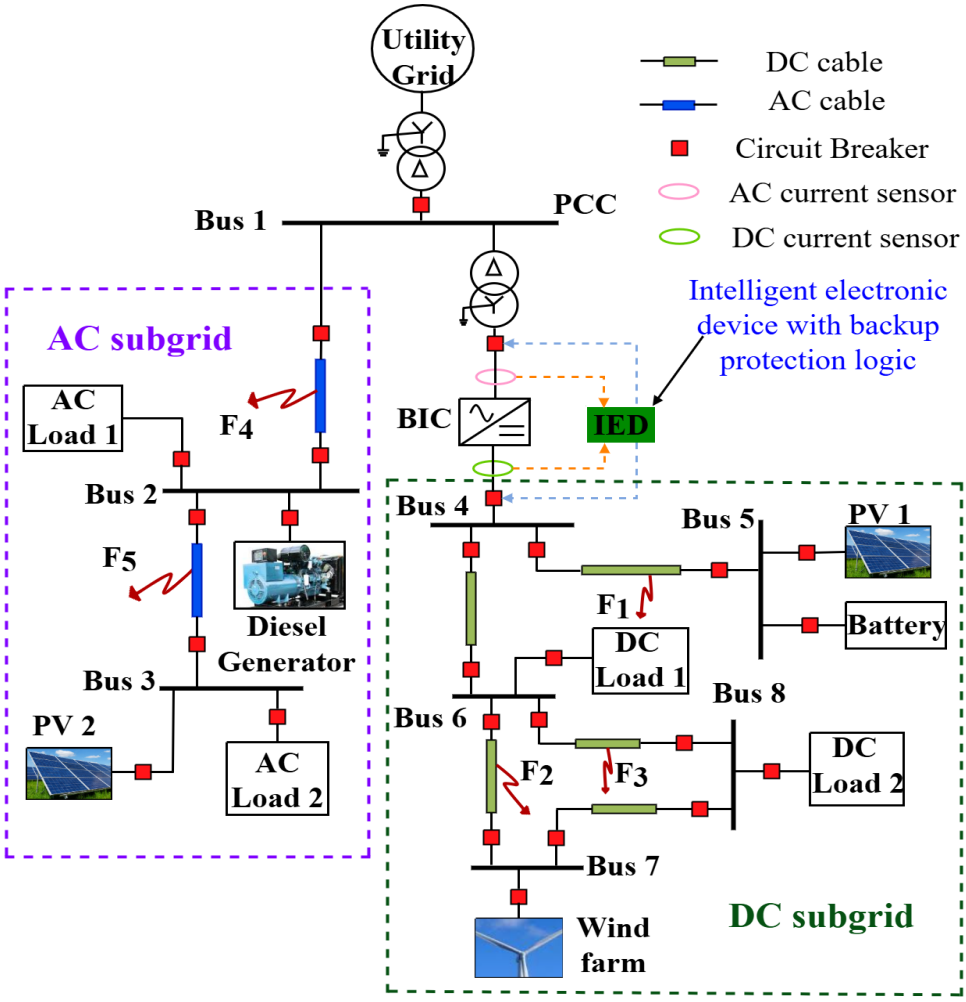

Figure 5.1: A hybrid AC-DC microgrid.

5.1 Introduction

In this chapter a time-domain backup protection for a hybrid AC-DC microgrid is proposed. The proposed scheme detect the fault and isolate the faulty subgrid from the PCC when primary protection fails. The scheme requires only currents at the AC and DC terminals of the BIC for the protection decision. One cycle moving average of the three-phase currents of the AC subgrid at the BIC terminal detects the ground faults in DC subgrids. The time span between two consecutive zero crossings of the phase currents and pre-fault DC current identifies the pole-to-pole fault. The superimposed component of mode-1 current at the DC terminal of the BIC is used to detect faults in the AC subgrid. The performance of the proposed method is validated with HIL simulation in real-time for AC and DC subgrid faults.

In this method, PGF, NGF, and PPF are the types of faults considered in the DC

Table 5.1: Rating of the hybrid AC-DC microgrid components [99, 115].

Components	**Ratings**
AC Grid VOltage (PCC)	4.16 kV
Transformer ratio	4.16kV/690V
DC Grid Voltage ($2V_c'$)	1.2 kV (± 600 V)
BIC	1 MW
PV 1 with DC-DC Converter	1 MW
PV 2	2 MW
PV 2 DC-AC Converter	2.5 MVA
Wind Turbine	2 MW PMSG
Wind VSC	2 MW
Diesel Generator	0.5 MVA
Battery	300 V, 1.3 kAh, 0.5 MW
Battery VSC	500 kW
DC Link Capacitance ($2C$)	25 mF
Cable Resistance	10 $m\Omega$/km/conductor
Cable Inductance	100 μH/km/conductor
Grounding Resistance (R_g)	0.05 Ω
AC Load 1 (Constant P,Q)	1 MVA at 0.88 power factor
AC Load 2 (Constant P,Q)	0.5 MVA at 0.88 power factor
DC Load	Constant Impedance (2 MW) and, Constant Power (1 MW)

subgrid of the hybrid microgrid. Similarly, single-line-to-ground (LG) fault, double-line-to-ground (LLG) fault, and three-phase (LLL) fault are considered in the AC subgrid of the system shown in Fig. 5.1. The rating of different components in the hybrid microgrid are given in Table 5.1.

5.2 Fault Analysis in Hybrid AC-DC microgrid

Hybrid AC-DC microgrids have complex fault behaviors due to the integration of power electronic converters, RES, and storage systems. Fault analysis helps in understanding different fault characteristics, enabling the design of effective protection schemes, ensuring converter safety, and improving system resilience.

This section describe the analysis of AC and DC subgrid faults in the hybrid AC-DC

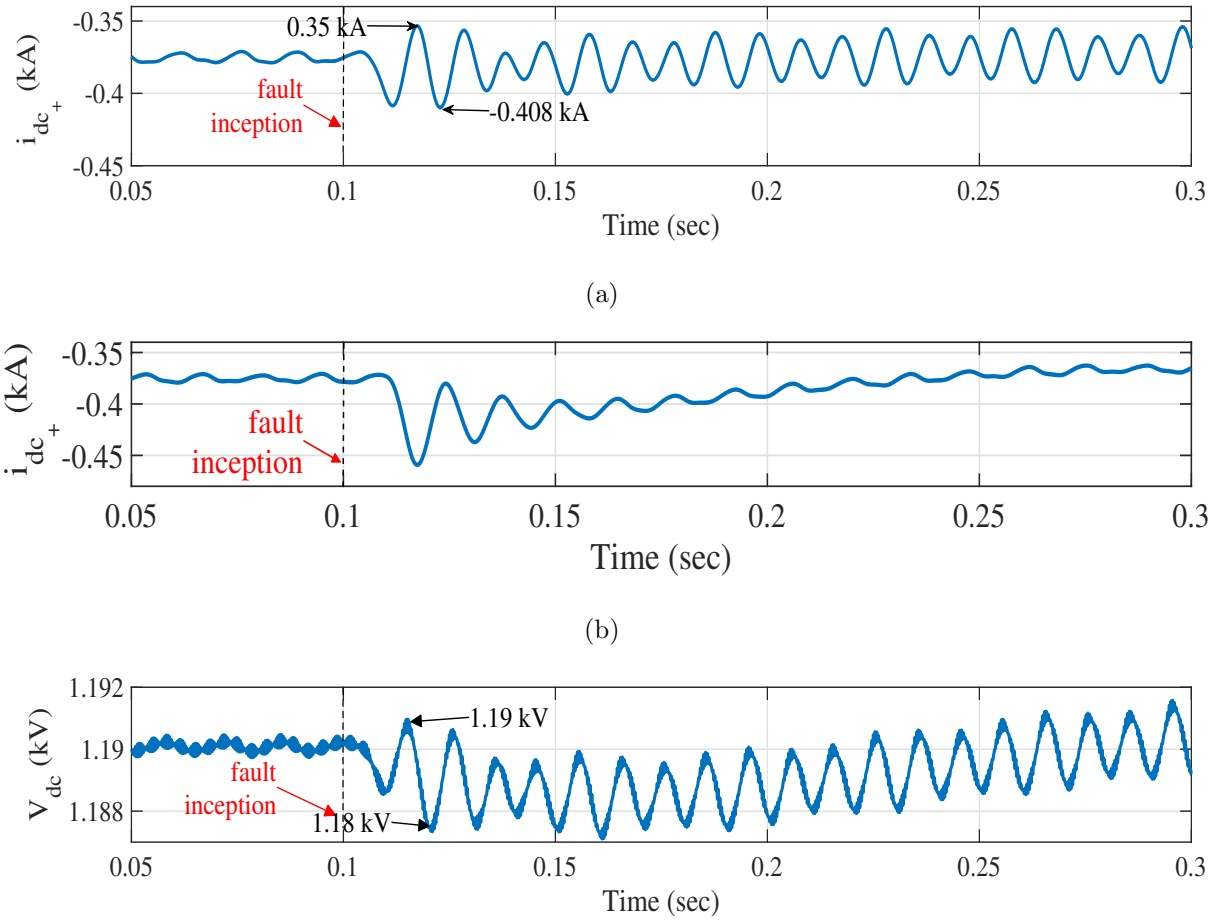

Figure 5.2: DC current of BIC during AC side faults (a) unsymmetrical fault (b) symmetrical fault (c) DC bus voltage during AC side unsymmetrical fault.

microgrid. Different faults in AC and DC subgrids are discussed one after another.

5.2.1 AC Subgrid Faults

5.2.1.1 Unsymmetrical fault

Consider an LG fault in the hybrid microgrid. During LG fault, the AC voltage at the converter terminal becomes unbalanced. These unbalanced three-phase voltages have different amplitudes and phase angles corresponding to phases a, b, and c. The direct axis component (v_d) of the three-phase voltages is given as:

$$\begin{aligned} v_d(t) = \frac{2}{3}[A_1 sin(\omega t + \phi_1)cos(\omega t) + A_2 sin(\omega t + \phi_2 - \frac{2\pi}{3}) \\ cos(\omega t - \frac{2\pi}{3}) + A_3 sin(\omega t + \phi_3 + \frac{2\pi}{3})cos(\omega t + \frac{2\pi}{3})] \end{aligned} \tag{5.1}$$

where, A_1, A_2, and A_3 are the peak amplitude of phase a, b, and c respectively, and ϕ_1, ϕ_2, ϕ_3 are the corresponding phase angles. Simplifying (5.1), it can be written as:

$$\begin{aligned} v_d(t) = \frac{1}{3}[\overbrace{A_1 sin(\phi_1) + A_2 sin(\phi_2) + A_3 sin(\phi_3)}^{DC\ Component} \\ + \overbrace{A_1 sin(2\omega t + \phi_1) + A_2 sin(2\omega t + \phi_2 - 4\pi/3)}^{Second\ Harmonic\ AC\ component} \\ \overbrace{+A_3 sin(2\omega t + \phi_3 + 4\pi/3)}^{Second\ Harmonic\ AC\ component}] \end{aligned} \tag{5.2}$$

From (5.2), it is clear that during an unsymmetrical fault (unbalanced condition), the second harmonic component is present in v_d along with the DC component.

5.2.1.2 Symmetrical fault

During a symmetrical fault on the AC side of hybrid microgrid, the second harmonic AC component in (5.2) will be zero, as ϕ_1, ϕ_2, and ϕ_3 are equal, and the peak amplitudes A_1, A_2, and A_3 are the same.

From the above, it is clear that any unbalance in the AC side causes the presence of a second harmonic component in v_d, and therefore, the active power of the BIC (P_{conv}) will have an oscillating component along with DC [127].

$$P_{conv} = 1.5(v_d i_d + v_q i_q) \tag{5.3}$$

Here, i_q will be zero as the converter is operating in DC bus voltage control mode. Following the power balance at the two sides of the BIC,

$$P_{AC} = P_{DC} + P_{2H} \tag{5.4}$$

The second harmonic active power component (P_{2H}) causes the oscillation in DC voltage and currents. Due to the large filter capacitance, the DC bus voltage has low oscillation amplitude as shown in Fig. 5.2, which may not be detected for high resistance fault. It is clear from Fig. 5.2 (a) and (c) that the oscillation in the DC side current of the BIC is higher than the DC voltage at the BIC terminal. The DC current varies from -0.408 kA to -0.350 kA, whereas the DC voltage variation is between 1.187 kV to 1.190 kV. For symmetrical fault in AC subgrid the oscillation in the DC terminal current of the BIC is

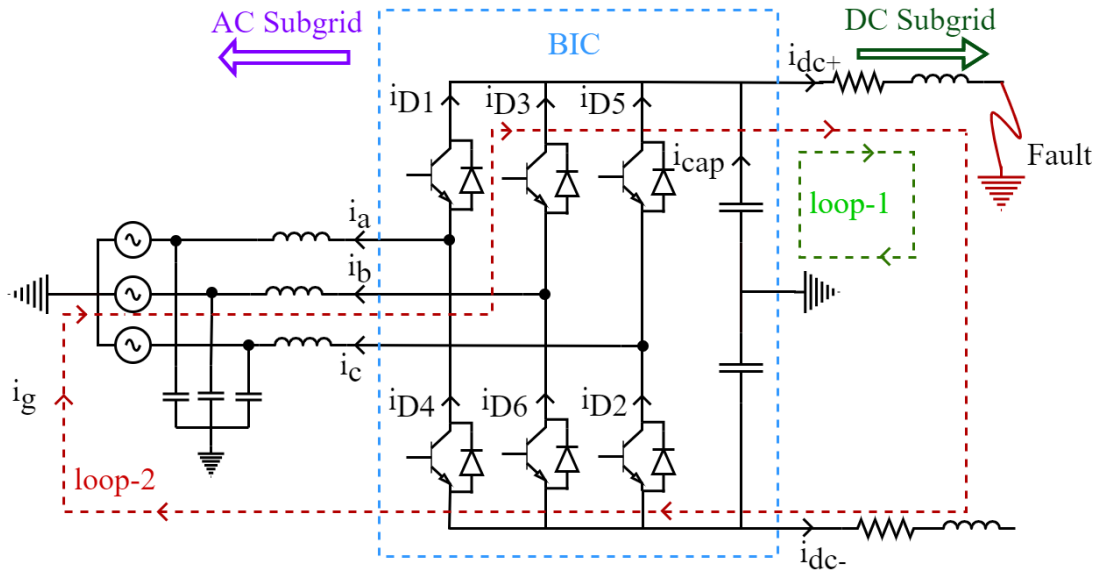

Figure 5.3: BIC during DC pole-to-ground fault.

not present which is shown in Fig. 5.2(b). Therefore, the DC current of BIC is considered as the decisive parameter for fault detection during AC faults.

5.2.2 DC subgrid Faults

5.2.2.1 Pole-to-ground fault

During a PGF, there are two fault loops, as shown in Fig. 5.3. Loop-1 is between the fault point and the grounded midpoint of the converter, and loop-2 is between the fault point and the grounding of the transformer. Due to the fault current in loop-2 (i_g), the freewheeling diodes in the upper-leg of the converter switches start conducting, providing a path to the i_g. In this case, the converter acts as an uncontrolled rectifier, and the fault current flows through the freewheeling diodes. Each diode in the upper-leg remains conducting during PGF. The total current in the upper switches of the bridge consists of both the currents from the AC subgrid and ground currents. Assuming the even distribution of the DC current through the diode branches of the converter, the currents through the upper switches can be given as

$$i_{D1}^{PGF} = \frac{i_g}{3} - i_a^{PGF}. \tag{5.5}$$

Similarly, $i_{D3}^{PGF} = \frac{i_g}{3} - i_b^{PGF}$, and $i_{D5}^{PGF} = \frac{i_g}{3} - i_c^{PGF}$. Here, i_a^{PGF}, i_b^{PGF}, and i_c^{PGF} are the sinusoidal components of fault currents in phase-a, b, and c, respectively during PGF. In

this case, the AC current also rise due to the shorting of the AC and DC terminals through freewheeling diodes. Assuming that the measured current at the BIC's AC terminal has a positive sign convention, as depicted in Fig 5.3. The AC current measured at the converter terminal, in this case, has a negative mean shift by the value equal to $\frac{i_g}{3}$ and can be given as

$$i_{a_{meas}}^{PGF}(t) = i_a^{PGF}(t) - \frac{i_g}{3}, \tag{5.6}$$

and shown in Fig. 5.4(a). Similar is true for phase-b and phase-c.

During an NGF, the freewheeling diodes in the lower-leg remain in conduction, and the AC current at the BIC terminal have a positive mean shift as shown in Fig. reffig4(b).

$$i_{a_{meas}}^{NGF}(t) = i_a^{NGF}(t) + \frac{i_g}{3} \tag{5.7}$$

Where, i_a^{NGF}, is the sinusoidal component of fault current in phase-a, during the NGF. It is clear from above that, during a ground fault in the DC subgrid, the current at the AC terminal of the BIC has a mean shift. During normal operation, the summation of three-phase instantaneous AC current will be zero (balanced condition). However, during ground faults in the DC subgrid, it has negative or positive non-zero values, depending on the PGF or NGF, respectively, as shown in Fig. 5.4(a) and (b).

5.2.2.2 Pole-to-pole fault

In the case of a PPF, the initial fault current is governed by the discharge of the DC link capacitor. When the capacitor voltage falls to zero, a large current flows through the DC cable and freewheeling diodes which is governed by the inductance in the fault loop. The currents through the converter legs in this case, assuming even distribution, can be given as:

$$\begin{cases} i_{D1}^{PPF} = \frac{i_{dc}^{PPF}}{3} - \frac{i_a^{PPF}}{2}, i_{D2}^{PPF} = \frac{i_{dc}^{PPF}}{3} + \frac{i_a^{PPF}}{2} \\ i_{D3}^{PPF} = \frac{i_{dc}^{PPF}}{3} - \frac{i_b^{PPF}}{2}, i_{D4}^{PPF} = \frac{i_{dc}^{PPF}}{3} + \frac{i_b^{PPF}}{2} \\ i_{D5}^{PPF} = \frac{i_{dc}^{PPF}}{3} - \frac{i_c^{PPF}}{2}, i_{D6}^{PPF} = \frac{i_{dc}^{PPF}}{3} + \frac{i_c^{PPF}}{2} \end{cases} \tag{5.8}$$

In this case, the interlink converter acts as a full-wave uncontrolled rectifier, contributing to the fault current from the AC subgrid of the hybrid microgrid, as shown in Fig. 5.4(c).

The peak value of i_{avg} for different DC subgrid faults are given in Table 5.2. It can be observed from Fig. 5.4 and Table 5.2 that, i_{avg} at the AC side of the BIC is negative

Table 5.2: Peak value of average current at AC side of BIC for different DC subgrid faults.

Fault Type	**PGF**	**NGF**	**PPF**
$i_{avg}(kA) = (i_a + i_b + i_c)/3$	-10.79	10.72	0.017

having peak of 10.79 kA during PGF in the DC subgrid. Similarly, in the case of NGF in the DC subgrid, i_{avg} is positive with a peak amplitude of 10.72 kA. On the other hand, for pole-to-pole fault in the DC subgrid, no mean shift in the AC side current is observed, and the average of the three-phase instantaneous current in this case is almost zero.

5.3 Proposed Protection Method

Based on the analysis in Section 5.2, the proposed method provides the backup protection of hybrid microgrid, explain as follows:

5.3.1 Backup Protection for DC subgrid Using AC side Current

The proposed method distinguished between AC and DC faults using the AC current of BIC. Before triggering the protection scheme, first the disturbance is to be identified by checking the condition given below [128]:

$$\psi = || \, i_p[n] - i_p[n-N] \, | - | \, i_p[n-N] - i_p[n-2N] \, || \geq 0.2 I_r. \tag{5.9}$$

where i_p and I_r represent the instantaneous and rated RMS value of phase current, respectively, n is the sample number, and N is the number of samples per cycle. A disturbance is detected when the condition in (5.9) satisfies for two consecutive samples.

5.3.1.1 Detection of DC ground faults

The three-phase currents at the AC terminal of BIC are sampled at a rate of 20 kHz, and one-cycle moving average of all the three-phase currents is obtained as:

$$i_{avg} = \frac{1}{N_T} \sum_{j=1}^{N_T} i_j \tag{5.10}$$

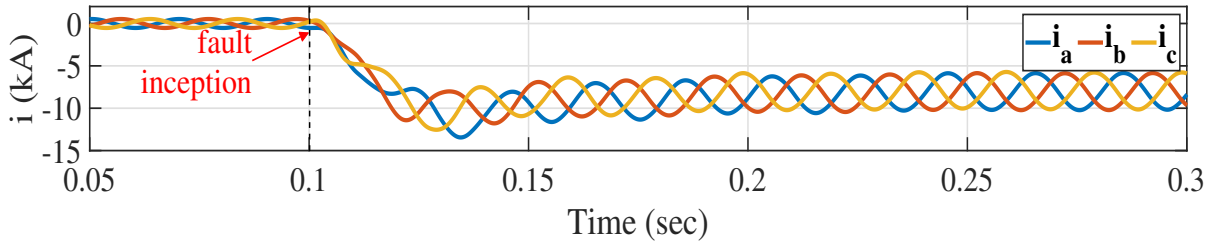

(a)

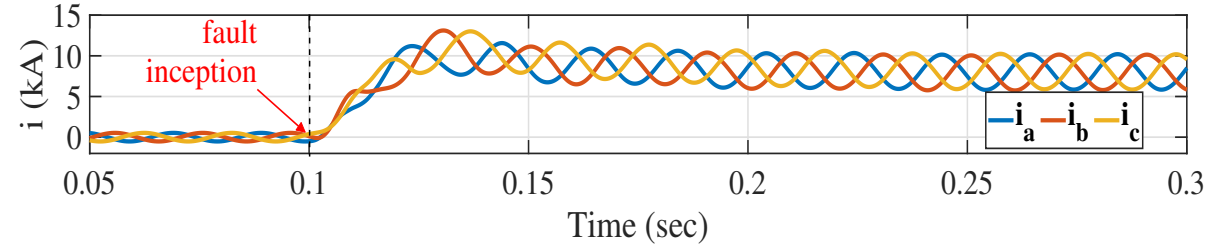

(b)

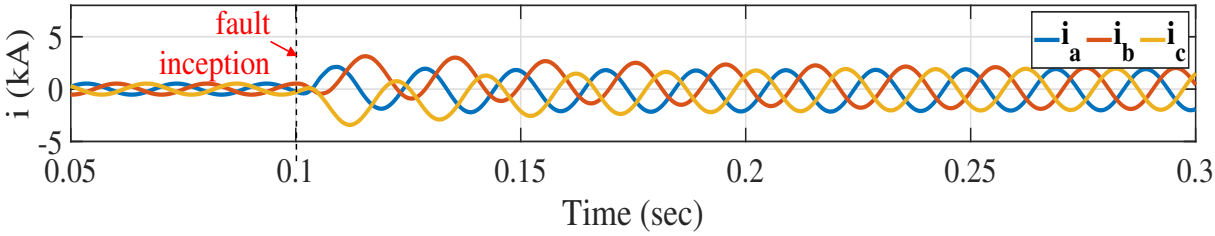

(c)

Figure 5.4: AC current at the BIC terminal during faults in the DC subgrid (a) PGF (b) NGF (c) PPF.

Here, i_{avg} is the one-cycle moving average of the AC current, and i_j is the current at j^{th} sample. During PGF, from (5.6) and (5.10), i_{avg} can be given as,

$$i_{avg}^{PGF}(t) = \frac{1}{N_T}\sum_{j=1}^{N_T}(i_j^{PGF} - \frac{i_{g_j}}{3}) \tag{5.11}$$

Since one-cycle moving average of sinusoidal current i^{PGF} will be zero, (5.11) can be written as:

$$i_{avg}^{PGF}(t) = \frac{1}{N_T}\sum_{j=1}^{N_T}(0 - \frac{i_{g_j}}{3}) \tag{5.12}$$

Therefore i_{avg}^{PGF} is negative for all the three phases a, b, and c. Similarly, in case of NGF, using (5.7) and (5.10)

$$i_{avg}^{NGF}(t) = \frac{1}{N_T}\sum_{j=1}^{N_T}(0 + \frac{i_{g_j}}{3}) \tag{5.13}$$

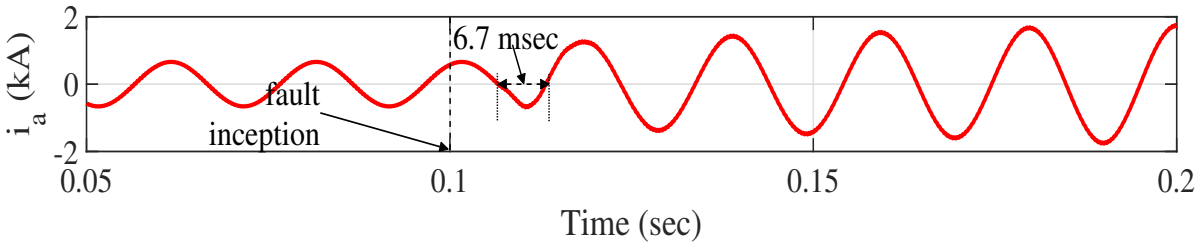

(a)

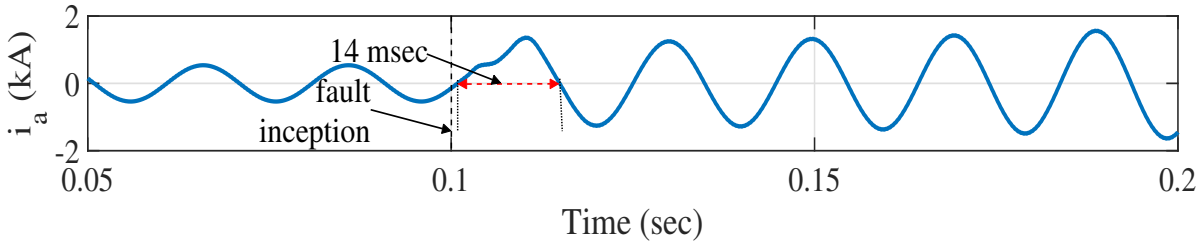

(b)

Figure 5.5: AC current at BIC terminal during AC faults (a) power flow from AC to DC (b) power flow from DC to AC.

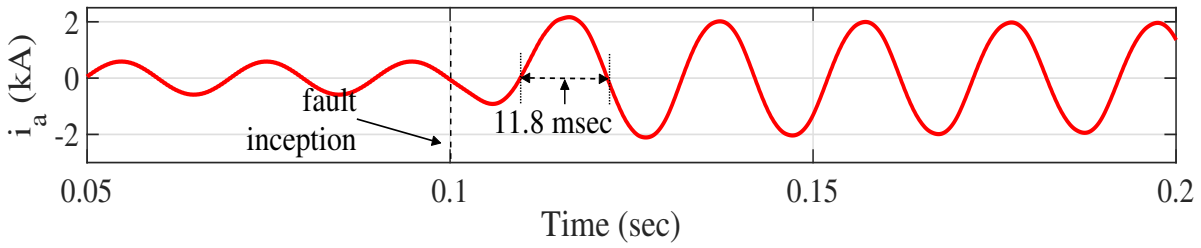

(a)

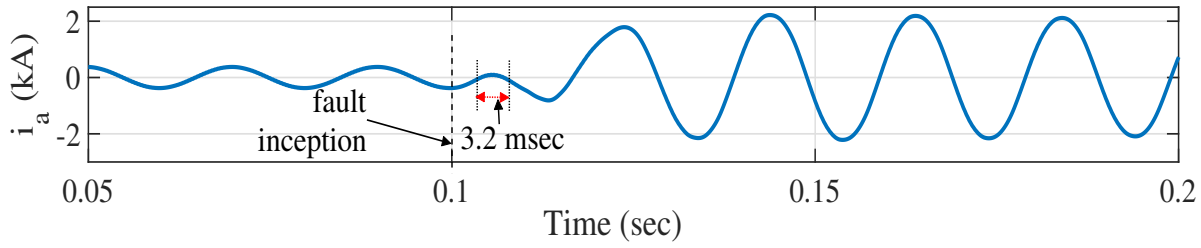

(b)

Figure 5.6: AC current at BIC terminal during DC PPF (a) power flow from AC to DC (b) power flow from DC to AC.

which is positive. Therefore, the negative value of i_{avg} for all the three-phase currents i_a, i_b, and i_c indicates a PGF, whereas the positive value of i_{avg} indicates an NGF.

5.3.1.2 Detection of DC pole-to-pole faults (PPF)

As shown in Fig. 5.4(c) and explained in Section 5.2.2, the AC current of BIC does not have a mean shift during PPF, and the BIC acts as a full wave uncontrolled rectifier contributing to the fault from AC subgrid. A similar situation also exists in the case of an AC fault, where the AC current have no mean shift. Therefore, to distinguish between AC faults and PPF in DC subgrid, the time span between two consecutive zero crossings (t_s) is measured and compared with the same during normal conditions, i.e., $T/2$, where T is the time period of the AC current. Since the fault inception near the zero crossing of a phase current may lead to a false decision [129]. Therefore, t_s is measured and compared with $T/2$ for all the three-phase currents to make the correct decision.

Consider the pre-fault power flow direction is from DC to AC subgrid. The pre-fault current at the AC terminal of BIC (I^{pre}) is in the direction as shown in Fig. 5.3. During a fault in the AC subgrid, the current measured at the BIC terminal (I^{AC}_{meas}) can be given as:

$$I^{AC}_{meas} = I^{pre} + I_F \tag{5.14}$$

Where I_F is the fault current from the DC subgrid. Similarly in case of a fault in the DC subgrid the measured current at BIC terminal I^{DC}_{meas} can be given as:

$$I^{DC}_{meas} = I^{pre} - I_R \tag{5.15}$$

here I_R is the fault current from the AC subgrid. The change in current due to fault in the AC or DC subgrid causes the change in the phase angle of currents measured at the BIC terminal. The phase change will be positive (counterclockwise) due to the fault in the DC subgrid and negative during the fault in the AC subgrid. The instantaneous phase change due to the fault causes the time-domain offset of the current. If the phase change is $\Delta\phi$, the time offset will be $\Delta t = \Delta\phi/\omega$ [129]. Similarly, when the pre-fault current is opposite to the direction shown in Fig. 5.3, the value of $\Delta\phi$ will be positive for fault in AC subgrid and negative during DC subgrid fault.

Fig. 5.5 shows the current at the AC terminal of BIC during a fault in the AC subgrid of the hybrid microgrid. It can be seen in Fig. 5.5(a) that two consecutive zero crossings cover a time span less than T/2 (= 10 msec during normal conditions for 50 Hz frequency) during AC fault when the power flow direction is from AC to DC. Similarly, when the power flow direction is reversed, the two consecutive zero crossings cover a time

Table 5.3: Fault direction using t_s and $i_{dc_+}^{pre}$.

	$t_s < T/2$	$t_s > T/2$
$i_{dc_+}^{pre} < 0$	DC side fault	AC side fault
$i_{dc_+}^{pre} > 0$	AC side fault	DC side fault

span more than T/2 during AC fault, as shown in Fig. 5.5(b). On the other hand, during PPF, t_s is more than T/2 for AC to DC power flow and less than T/2 for DC to AC power flow, as shown in Fig. 5.6 (a) and (b), respectively.

From Fig. 5.5 and 5.6, it is clear that the power flow direction affects the time span between two consecutive zero crossings during faults. Therefore, a flag is set using the pre-fault DC current of the BIC, which indicates the pre-fault power flow direction. Using the power flow direction flag and time span between two consecutive zero crossings, the PPF is detected, as shown in Fig. 5.7.

Using t_s with pre-fault power flow direction ($i_{dc_+}^{pre}$), the AC and DC subgrid faults can be distinguished. Decision will be made when all three phase currents satisfy the conditions mentioned in Table 5.3.

5.3.2 Backup Protection of the AC subgrid Using DC Current

Any disturbance on either subgrid of the hybrid microgrid causes a high rate of change of current (ξ) at the DC terminal of BIC. However, under steady state, ξ is close to zero. Therefore ξ is considered as the criterion for triggering the main algorithm, which is given as

$$\xi = \frac{1}{\Delta t}\left(\sum_{j=1}^{N} |i_{j+1} - i_j|\right) \tag{5.16}$$

where i_j is the current of j^{th} sample, Δt is the sampling interval, and M is the number of samples in a data window. The protection starts when ξ exceeds the threshold (k). In this study, M = 10 for 20 kHz sampling frequency and $k = 6.2$ kA/sec.

Positive and negative pole currents at the BIC terminal are used to distinguish between the faults in AC and DC subgrids. The symmetrical component decomposition [130] of the pole domain DC current at the BIC terminal is obtained to find the mode-1

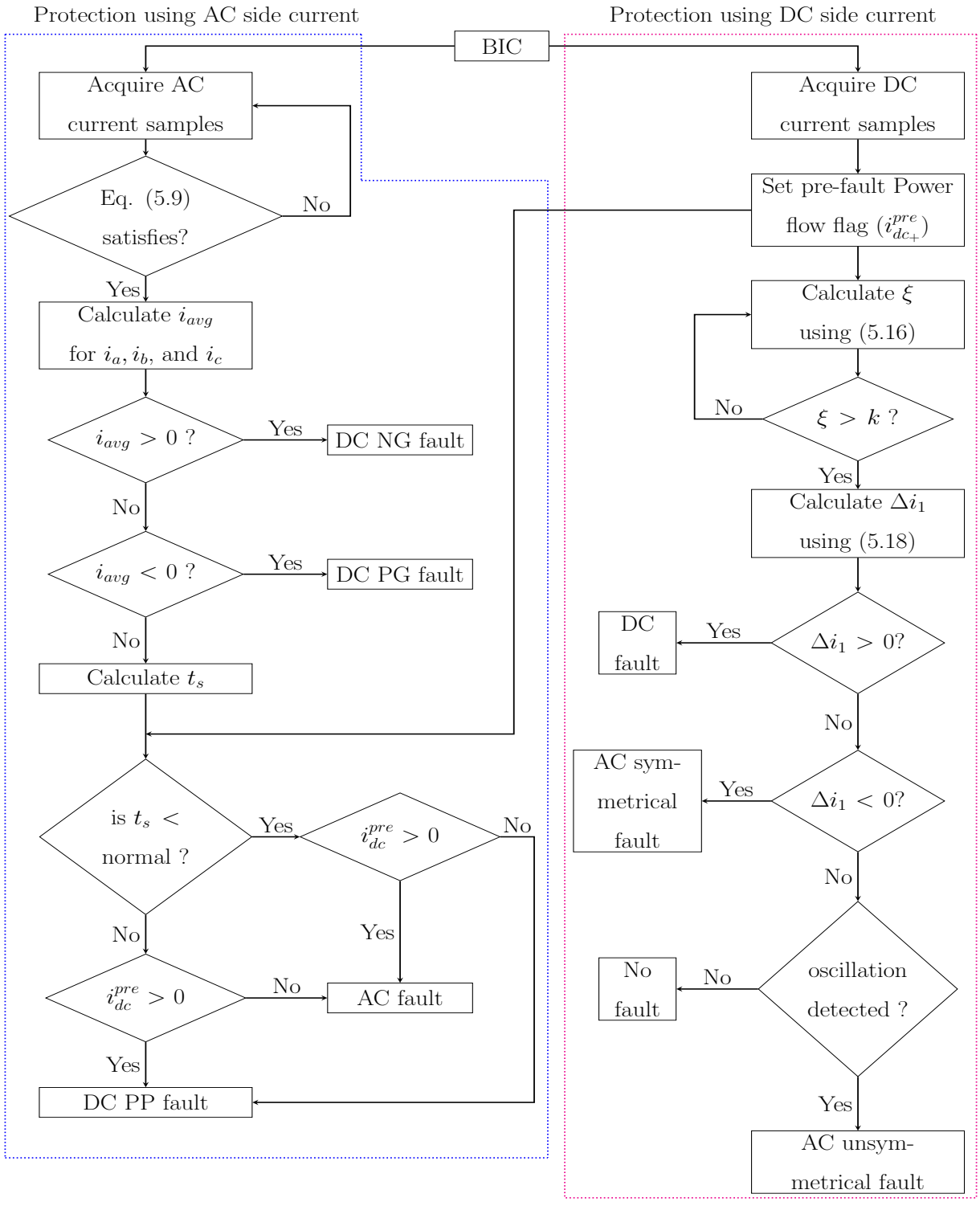

Figure 5.7: Flow chart of the proposed method.

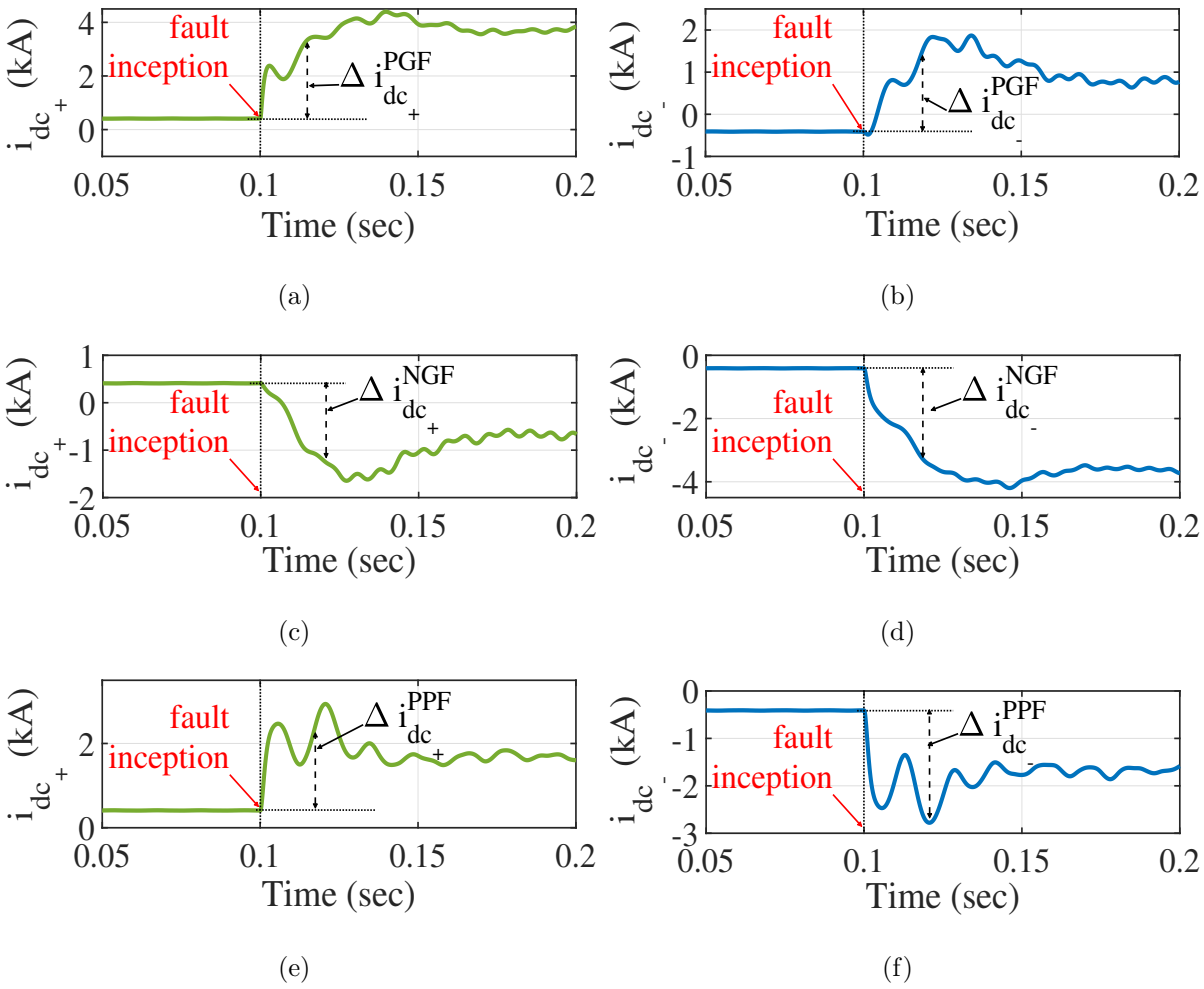

Figure 5.8: DC current at BIC terminal during faults in DC subgrid (a) $i_{dc_+}^{PGF}$ (b) $i_{dc_-}^{PGF}$ (c) $i_{dc_+}^{NGF}$ (d) $i_{dc_-}^{NGF}$ (e) $i_{dc_+}^{PPF}$, and (f) $i_{dc_-}^{PPF}$.

and mode-0 currents, as shown in (5.17).

$$\begin{bmatrix} i_1 \\ i_0 \end{bmatrix} = \begin{bmatrix} 1 & -1 \\ 1 & 1 \end{bmatrix} \begin{bmatrix} i_{dc_+} \\ i_{dc_-} \end{bmatrix} \tag{5.17}$$

where i_1, and i_0 are the mode-1 and mode-0 currents, respectively, in the modal-domain and, i_{dc_+}, and i_{dc_-} are the positive-pole and negative-pole currents, respectively in pole-domain.

The superimposed component of mode-1 current (Δi_1) is calculated using pre-fault (i_1^{pre}) and post-fault (i_1^f) values of i_1 to distinguish between faults in AC and DC subgrids . Δi_1 is given as:

$$\Delta i_1(t) = i_1^f(t) - i_1^{pre}(t) \tag{5.18}$$

5.3.2.1 Detection of AC symmetrical faults

As explained in Section 5.2.1, during symmetrical faults in the AC subgrid, the second harmonic component will be zero, and the DC current at the BIC has no sustained oscillations. A similar case also arises during faults in the DC subgrid. Therefore, it is necessary to distinguish between AC symmetrical faults and DC faults. During fault in the DC subgrid (consider PGF), the fault current seen by the positive pole sensor at the DC terminal of BIC is given as [49],

$$i_{dc_+}^{PGF}(t) = \frac{v_C'(0)}{R_1}\left(1 - e^{-\frac{R_1}{L_1}t}\right) + \frac{v_C'(0)}{L_1(s_2 - s_1)}[e^{-s_1 t} - e^{-s_2 t}] \tag{5.19}$$

where, $s_1, s_2 = \frac{R_1}{L_1} \pm \sqrt{\left(\frac{R_1}{L_1}\right)^2 - \frac{1}{L_1 C_{eq}}}$. R_1 and L_1 are the equivalent resistance and inductance, respectively in the fault loop. $v_c'(0)$ is the pre-fault voltage across the equivalent capacitance (C_{eq}) in the fault loop.

In this case, the positive pole superimposed current at BIC terminal (Δi_{dc_+}) is obtained as

$$\Delta i_{dc_+}^{PGF}(t) = i_{dc_+}^{PGF}(t) - i_{dc_+}^{pre} \tag{5.20}$$

where, $i_{dc_+}^{pre} = \frac{v_C'(0)}{R_{eq}}$ and $R_{eq} = R_{line} + R_{load}$. The pre-fault negative pole current ($i_{dc_-}^{pre}$) will be opposite to that of ($i_{dc_+}^{pre}$). In the case of a PGF, being a bi-polar DC system, the healthy pole (negative pole in this case) continues the power supply to the load. Therefore, the negative pole current during PFG ($i_{dc_-}^{PGF}$) is reversed and becomes positive. The superimposed negative pole current, in this case, can be given as:

$$\Delta i_{dc_-}^{PGF}(t) = i_{dc_-}^{PGF}(t) - (-i_{dc_+}^{pre}) \tag{5.21}$$

So, during PGF $\Delta i_{dc_-}^{PGF}$ is also positive. However, being a faulty pole, the value of $\Delta i_{dc_+}^{PGF}$ will be higher than that of $\Delta i_{dc_-}^{PGF}$, as shown in Fig. 5.8(a) and (b), respectively, and the value of Δi_1 during PGF,

$$\Delta i_1^{PGF} = \Delta i_{dc_+}^{PGF}(t) - \Delta i_{dc_-}^{PGF}(t) \tag{5.22}$$

will be positive.

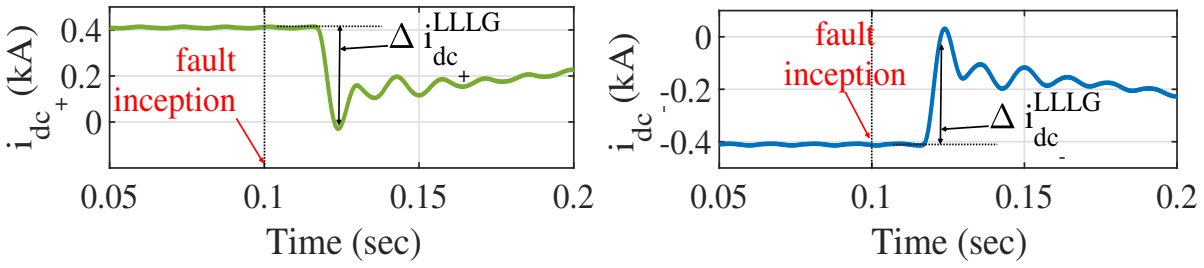

(a) (b)

Figure 5.9: DC current at BIC terminal during symmetrical faults in the AC subgrid (a) $i_{dc_+}^{LLLG}$ (b) $i_{dc_-}^{LLLG}$.

Similarly, during NGF, the positive pole superimposed current ($\Delta i_{dc_+}^{NGF}$) and negative pole superimposed current ($\Delta i_{dc_-}^{NGF}$) both are negative as shown in Fig. 5.8 (c) and (d), respectively. Being a faulty pole, the value of $\Delta i_{dc_-}^{NGF}$ is more than that of $\Delta i_{dc_+}^{PGF}$ and therefore, Δi_1 in this case,

$$\Delta i_1^{NGF} = (-\Delta i_{dc_+}^{NGF}(t)) - (-\Delta i_{dc_-}^{NGF}(t)) \tag{5.23}$$

will remain positive.

During PPF, both the i_{dc_+}, and i_{dc_-} increases in their respective pre-fault direction as shown in Fig. 5.8(e) and (f) respectively. In this case, $\Delta i_{dc_+}^{PPF}$ will be positive and, $\Delta i_{dc_-}^{PPF}$ will be negative, that lead to the positive Δi_1^{PPF}.

However, during symmetrical fault (LLLG) in the AC subgrid, the fault current seen by the positive pole ($i_{dc_+}^{LLLG}$) and negative pole ($i_{dc_-}^{LLLG}$) sensors at the DC terminal of BIC will be opposite to that of ($i_{dc_+}^{PPF}$) and ($i_{dc_-}^{PPF}$), respectively. Therefore, $\Delta i_{dc_+}^{LLLG}$ will be negative, and $\Delta i_{dc_-}^{LLLG}$ will become positive as shown in Fig. 5.9(a), and (b) respectively. Therefore, Δi_1^{LLLG} will be negative in this case.

5.3.2.2 Detection of AC unsymmetrical faults

As explained in Section 5.2.1, the DC current of the BIC has sustained oscillation of the second harmonic component. The oscillation also persists in i_1, and Δi_1 has multiple zero crossings during unsymmetrical faults in the AC subgrid. By detecting the zero crossings in Δi_1 the AC unsymmetrical faults can be detected.

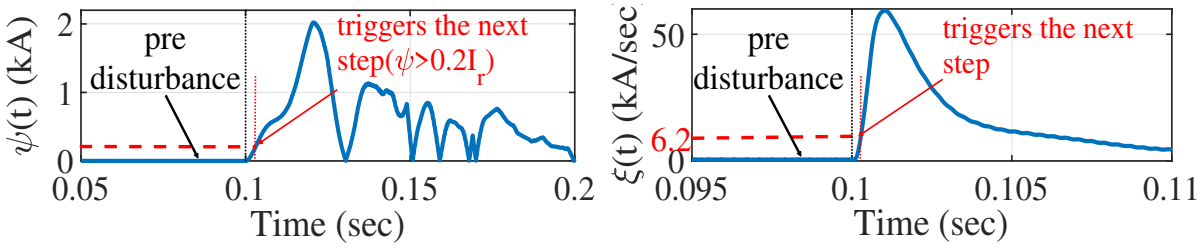

(a) (b)

Figure 5.10: Disturbance detection parameters at BIC terminals (a) ψ (for AC current) (b) ξ (for DC current).

5.4 Performance Evaluation

The performance of the proposed method is validated on the test system shown in Fig. 5.1, which is simulated using RTDS. Different AC and DC faults at different locations are simulated, and the performance of the proposed schemes is validated, considering AC and DC current of the BIC. Data are extracted with the sampling frequency (f_s) of 20 kHz, and the fault inception time is 0.1 sec for all cases.

Before identifying the faulted subgrid, it is necessary to detect the presence of disturbance. For this purpose, (5.9) and (5.16) need to be satisfied using the AC and DC current, respectively. Figure 5.10 (a) and (b) show the disturbance detection parameters using AC and DC current, respectively.

5.4.0.1 PGF in DC subgrid

A PGF, F_1 shown in Fig. 5.1 is simulated in the line segment between bus-4 and bus-5 with a fault resistance (R_f) of 0.1 Ω. The simulation results in Fig. 5.11(a) shows i_1 during PGF. It is clear from Fig. 5.11(a) that, during F_1, the value of i_1 increases in the positive direction, and therefore Δi_1 is positive.

Similarly, the AC current of the BIC are analyzed during F_1 and, the average (i_{avg}) of three phase currents i_a, i_b, and i_c are calculated as per (5.10). Fig. 5.11(b) shows that during F_1, the value of i_{avg} becomes negative, and therefore, the fault can be detected as a PG fault in the DC subgrid.

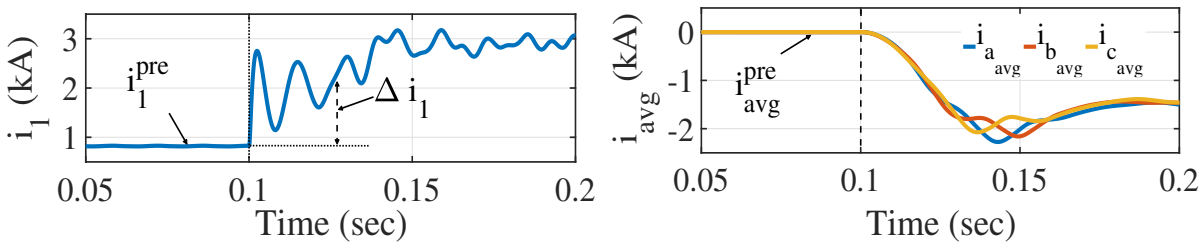

(a) (b)

Figure 5.11: AC and DC current at BIC terminals during PG fault in the DC subgrid (a) i_1 (b) i_{avg}.

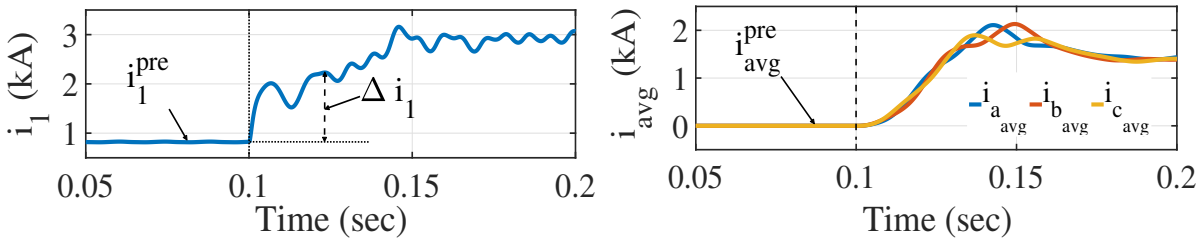

(a) (b)

Figure 5.12: AC and DC current at BIC terminals during NG fault in the DC subgrid (a) i_1 (b) i_{avg}.

5.4.0.2 NGF in DC subgrid

An NGF, (F_2 in Fig. 5.1) is simulated in the line segment between bus-6 and bus-7 with $R_f = 0.1\ \Omega$. The simulation results are shown in Fig. 5.12. It is clear from Fig. 5.12(a) that, the value of i_1 increases in the positive direction, and therefore Δi_1 is positive, and the NGF in the DC subgrid is confirmed.

Similarly, it is clear from Fig. 5.12(b) that, during F_2, the value of i_{avg} becomes positive, and the fault is confirmed as NG fault in the DC subgrid.

5.4.0.3 PPF in DC subgrid

Figure 5.13(a) shows the simulation results for a PP fault (F_3 in Fig. 5.1), simulated in the line segment between bus-6 and bus-8 with $R_f = 0.1\ \Omega$. It is clear from Fig. 5.13(a) that the value of i_1 increases in the positive direction, and therefore Δi_1 is positive. Figure 5.13(b), (c) and (d) shows the three-phase currents i_a, i_b, and i_c, respectively at the AC terminals of the BIC during F_3, when pre-fault power flow direction is from AC to DC

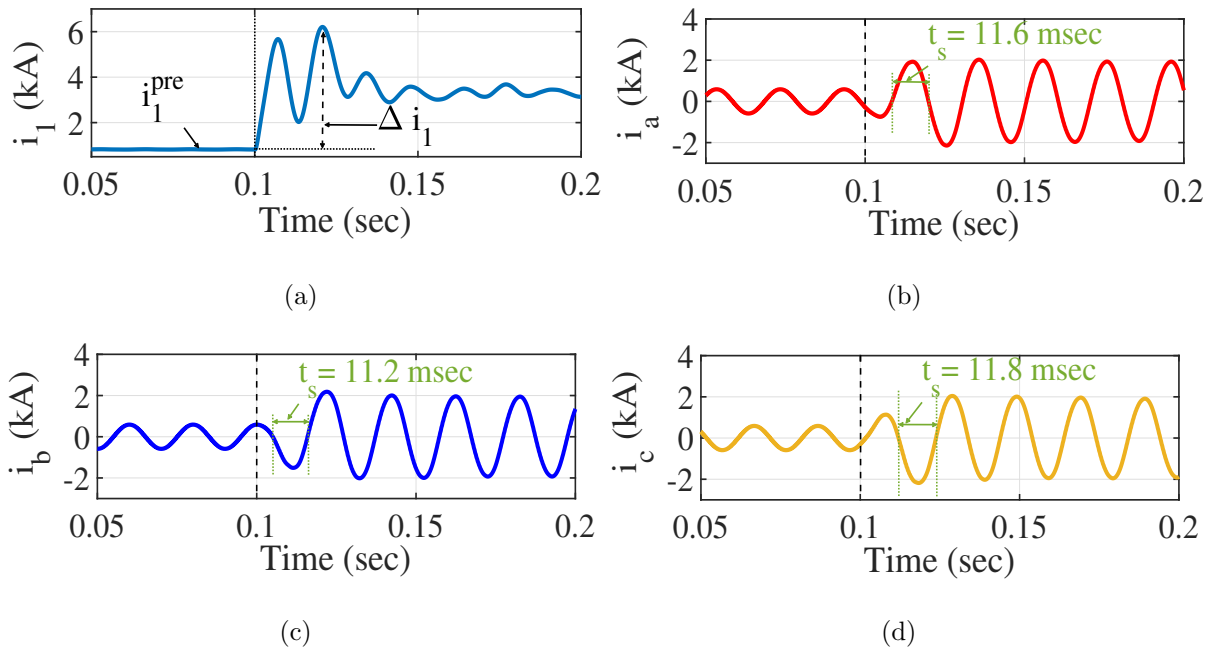

Figure 5.13: AC and DC side currents at BIC terminals during DC side PP fault (a) i_1 (b) i_a (c) i_b (d) i_c.

subgrid. It is clear that during (F_3), the time span between two consecutive zero crossings (t_s) increases at the fault inception. Since the pre-fault power flow direction is from the AC to the DC, the increase in t_s confirms the PPF in the DC subgrid.

5.4.0.4 Symmetrical faults in the AC subgrid

A LLLG fault in the AC subgrid is simulated in the line section between bus-1 and bus-2 (F_4 in Fig. 5.1). The simulation results in Fig 5.14(a) show that, during F_4, the value of l_{line} increases in the negative direction and therefore Δi_1 will be negative.

Simulation results shown in Fig. 5.14(b), (c), and (d) indicate the reduction in t_s for the AC current i_a, i_b, and i_c, respectively. Being the pre-fault power flow from AC to DC subgrid of hybrid microgrid, the value of t_s less than 20 msec (normal value of t_s for 50 Hz) indicates the fault in AC subgrid.

5.4.0.5 Unsymmetrical faults in the AC subgrid

A LLG fault in the line section between bus-2 and bus-3 (F_4 in Fig. 5.1) is simulated with $R_f = 0.1\ \Omega$. The simulation results are shown in Fig. 5.15. It is clear from Fig. reffig12(a) that during LL-G fault in the AC subgrid, i_1 oscillates at a frequency of 100

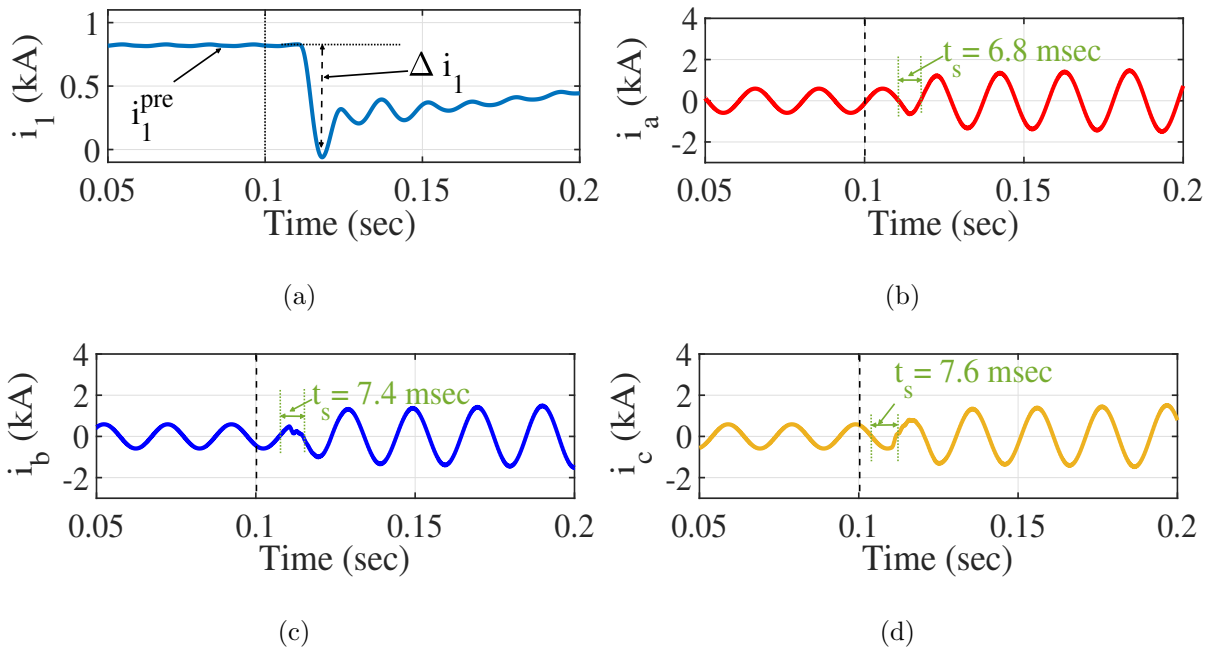

Figure 5.14: DC and AC current at BIC terminals during symmetrical fault in the AC subgrid (a) i_1 (b) i_a (c) i_b (d) i_c .

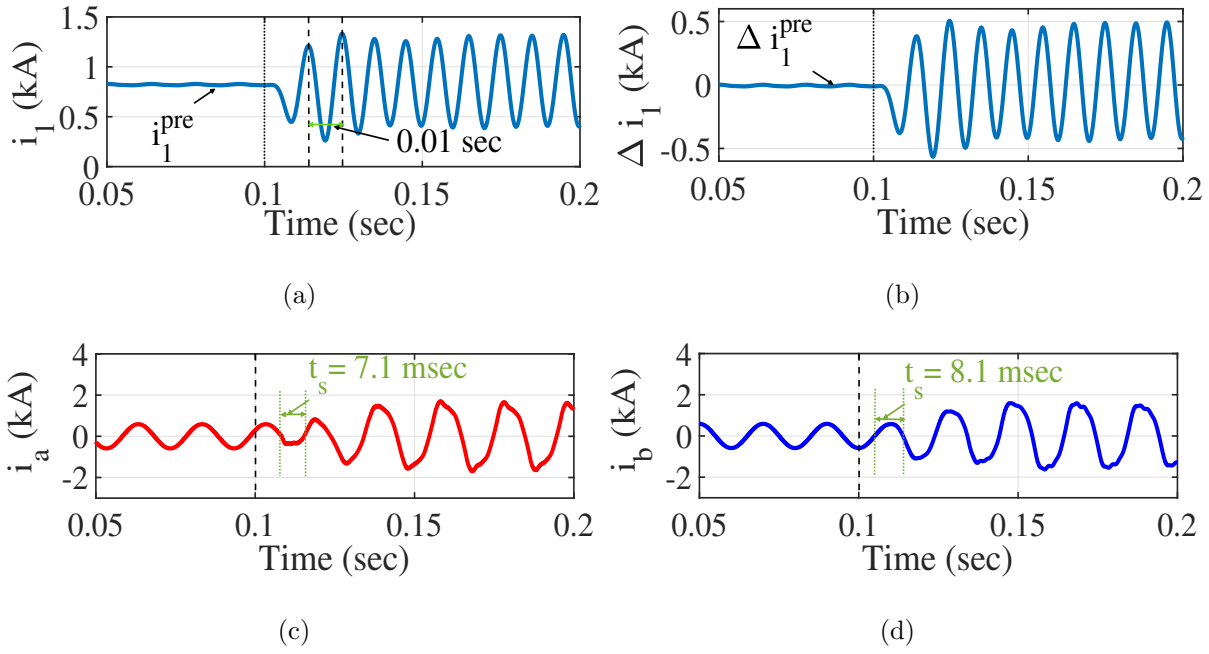

Figure 5.15: DC and AC current at BIC terminals during unsymmetrical fault in the AC subgrid (a) i_1 (b) Δi_1 (c) i_a (d) i_b .

Hz (second harmonic component to the fundamental frequency of 50 Hz), that confirms the presence of unsymmetrical faults in the AC subgrid. Figure 5.15 (c) and (d) show the

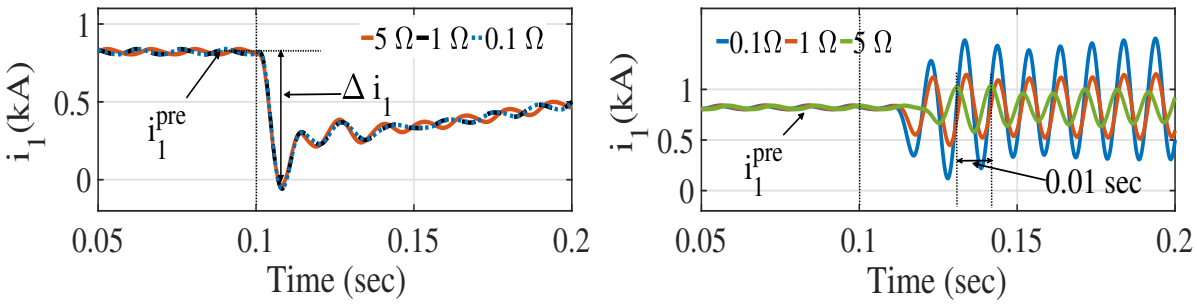

(a) (b)

Figure 5.16: Mode-1 current at DC terminal of BIC for fault on AC subgrid with different fault resistance (a) Symmetrical Fault (b) Unsymmetrical (LG) Fault.

AC current at the BIC terminal corresponding to the faulted phase. It is clear that the value of t_s reduces and becomes 17.1 msec and 18.1 msec for i_a and i_b phases, respectively. Since the pre-fault power flow direction is from the AC to the DC subgrid, the reduced value of t_s indicates a fault in the AC subgrid.

5.5 Sensitivity of the Proposed Scheme for High Resistance Faults

To verify the sensitivity of the proposed scheme, different faults in both the AC and DC subgrids of the microgrid are simulated with different fault resistance. Both, symmetrical (F_4 in Fig. 5.1) and asymmetrical (F_5 in Fig. 5.1) faults in the AC subgrid is simulated with fault resistance varying from 0.1 Ω to 5 Ω. The value of mode-1 current at DC terminal of the BIC is calculated for each case and shown in Fig. 5.16 (a) and (b) respectively. It is clear from Fig. 5.16 (a), that the change in mode-1 current (Δi_1) is negative enough to detect the fault even for fault resistance value of 5 Ω . Similarly, for unsymmetrical fault in the AC subgrid the oscillation is observed in mode-1 current at the DC terminal of BIC as given in Fig. 5.16(b).

Similar to AC subgrid faults, the sensitivity of the proposed method is also verified for faults at different locations in the DC subgrid with varying fault resistance. A PGF (F_2 in Fig. 5.1) is simulated with different fault resistance from 1 Ω to 5 Ω. The instantaneous average value of three-phase currents at the BIC terminal is calculated for each

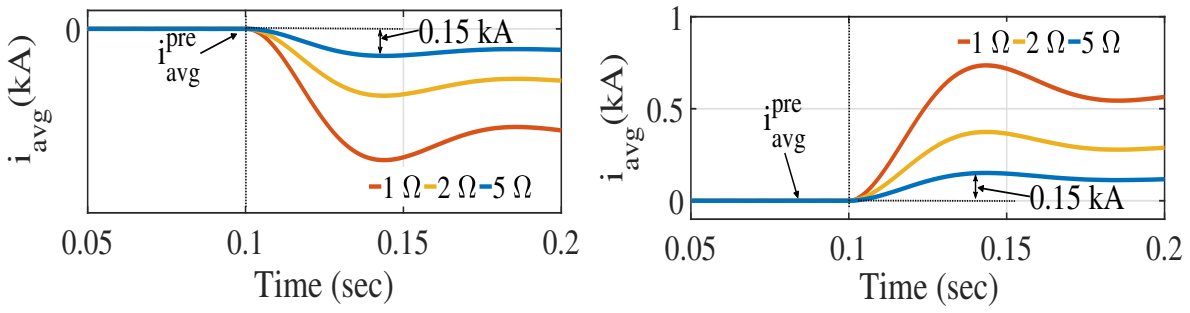

(a) (b)

Figure 5.17: Instantaneous average of three-phase currents at AC terminal of BIC for fault on DC subgrid with different fault resistance (a) Positive pole-to-ground fault (b) Negative pole-to-ground fault.

case and shown in Fig. 5.17 (a). Similarly, an NGF (F_1 in Fig. 5.1) is simulated with fault resistance varying from 1 Ω to 5 Ω. It is clear from Fig. 5.17 (a) and (b), that the proposed backup protection using AC current can detect high resistance ground faults in the DC subgrid.

It can be concluded from Fig. 5.16 and Fig. 5.17 that the proposed method has high sensitivity with varying fault resistance and fault locations.

Further, the change in the filter inductance of BIC also affect the sensitivity of the proposed scheme (in case of PPF in the DC subgrid), however the filter inductance if fixed at the stage of system design and will not change with fault.

5.6 Hardware Validation of the Proposed Scheme in Real-Time

HIL validation plays a vital role in the development and testing of protection schemes for modern power systems, especially for DC microgrids and hybrid AC-DC networks. It bridges the gap between pure software simulation and real-world deployment by allowing real-time interaction between physical hardware (e.g., relays, controllers) and a simulated power system environment.

A control hardware-in-loop (CHIL) validation of the proposed method is conducted using RTDS with C2000 series (tms320f28379d) digital signal processor (DSP) to validate

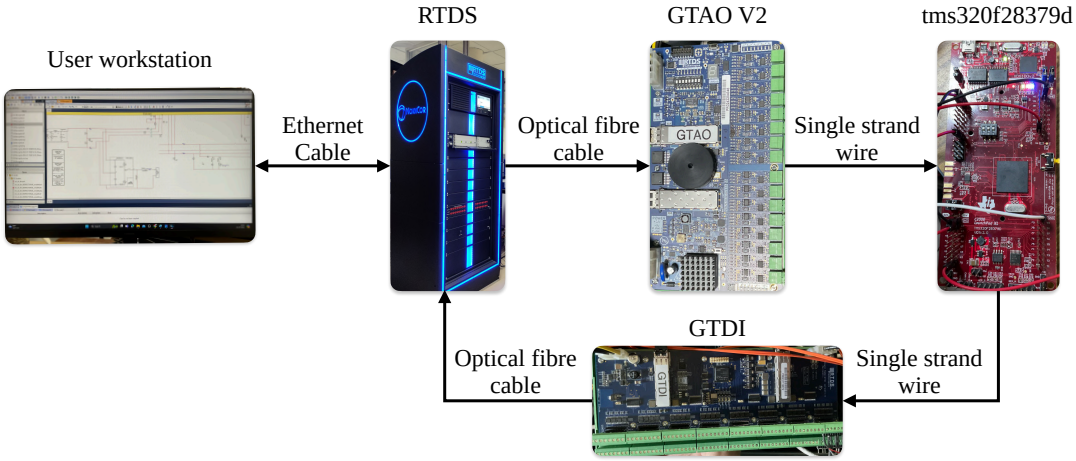

Figure 5.18: Schematic for the HIL validation of the proposed scheme.

the performance of the proposed scheme. The current from the RTDS is fed to the analog-to-digital converter (ADC) pins of the DSP through gigabit transceiver analog output card version-2 (GTAO V2) using a single-strand wire. The proposed protection algorithm is implemented in the DSP card using Code Composer Studio and MATLAB. Further, the trip signal (Digital output) from the DSP is given to the gigabit transceiver digital input (GTDI) card of the RTDS through the general purpose input/output (GPIO) pin of the DSP to form a closed-loop and opens the breaker as shown in Fig. 5.18. The trip signal is also taken out to the digital signal oscilloscope (DSO) using the digital-to-analog converter (DAC) pin of the DSP, as shown in Fig. 5.19.

5.7 Operating Time of the Proposed Scheme

The operating time of the proposed scheme is compared in both the hardware environment (using DSP) and the simulation environment (using RTDS). In the hardware environment, the operating time is 19 msec in case of fault detection in the DC subgrid using the AC current of the BIC, as shown in Fig. 5.20(a). When DC current of the BIC are used for fault detection in the AC subgrid, the operating time is 46.3 msec, as shown in Fig. 5.20(b). Further, in the simulation using RTDS, the operating time is 10.8 msec in the case of DC subgrid fault detection using the AC current of the BIC and 24.4 msec for AC subgrid fault detection using the DC current of the BIC, as shown in Fig. 5.21 (a) and

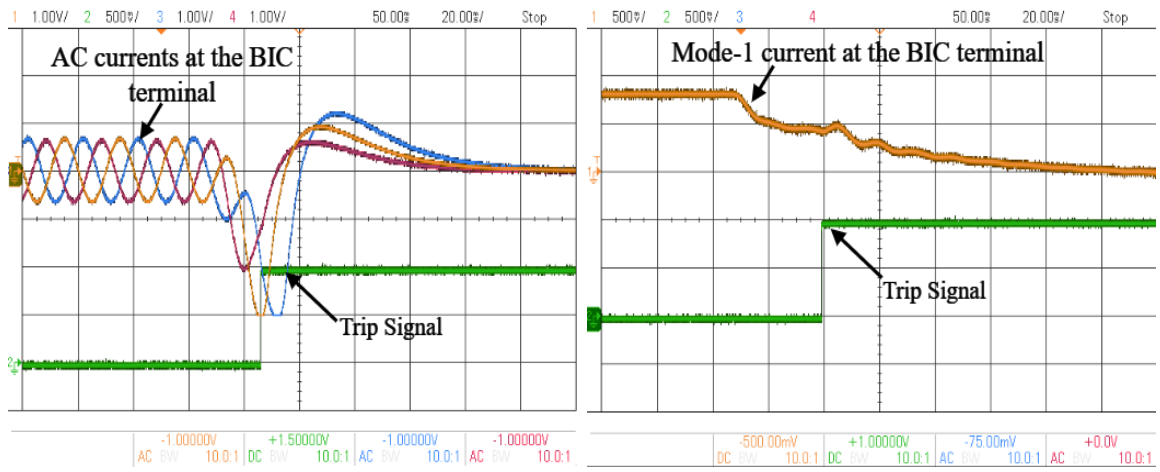

(a) (b)

Figure 5.19: Performance of the proposed method in CHIL (a) protection using AC current of BIC (b) protection using DC current of the BIC.

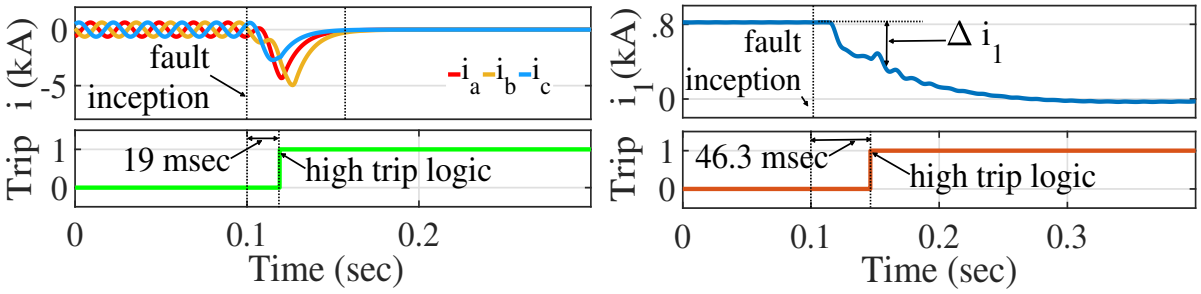

(a) (b)

Figure 5.20: Operating time of the proposed scheme with CHIL (a) protection using AC current of BIC (b) protection using DC current of BIC.

Fig. 5.21 (b), respectively.

It is worth mentioning that the operating time of the proposed protection method depends on the primary protection operating time ($t_{primary}$) for the corresponding subgrid. Therefore, an intentional time delay is required in the proposed backup protection method to coordinate with primary protection. The operating time for the backup protection (t_{backup}) can be given as:

$$t_{\text{backup}} = t_{\text{primary}} + \text{CTI} + t_{\text{CB}} \tag{5.24}$$

Here, CTI is the coordination time interval between primary and backup protection, and t_{CB} is the breaker opening time for primary protection.

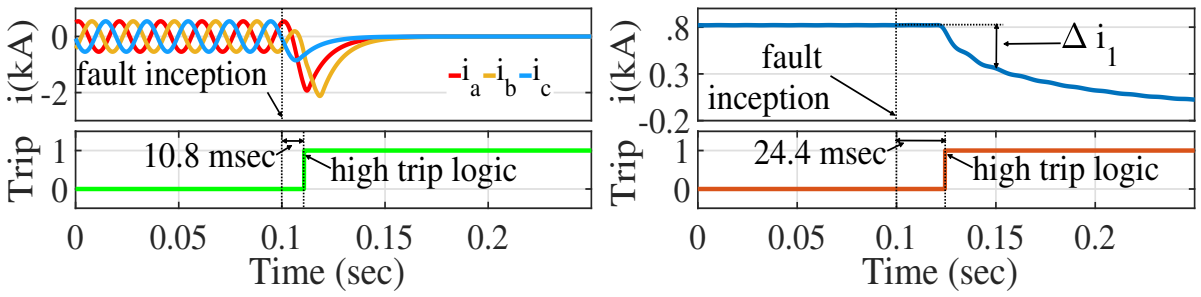

(a) (b)

Figure 5.21: Operating time of the proposed scheme with RTDS (a) protection using AC current of BIC (b) protection using DC current of BIC.

The coordination between primary and backup protection is shown in Fig. 5.22 for both, the AC and DC subgrid faults. A PGF (F_1 in Fig. 5.1) is simulated in the DC subgrid. The protection scheme in [48] is considered as the primary protection in this case. As shown in Fig. 5.22(a) the trip signal from primary protection scheme is generated within 1 msec. However, due to breaker failure, the fault is still remains in the system and the current (i_{4-5}) further increased. The backup protection detects the fault and generates the trip signal to open the breaker at the PCC. The time difference between primary and backup protection in this case is 9.4 msec.

Similarly, an unsymmetrical fault (F_4 in Fig. 5.1) is simulated in AC subgrid. The trip signal ($Trip_{primary}$) is generated by the primary protection but due to breaker failure, the fault is not isolated. The oscillation in mode-1 current (i_1) can be seen in Fig. 5.22 (b) and therefore the backup protection generates the trip signal to open the breaker at PCC.

It is required to mention that the primary protection operating time may vary depending on the protection method, therefore the intentional wait time for the backup protection needs to be adjusted as per the requirement.

5.8 Comparison with Available Methods

The proposed method is compared with the existing backup protection techniques, summarized in Table 5.4. The methods presented in [27, 28, 103, 104] are compared with the proposed scheme in terms of considered microgrid topology, signal requirement, fault

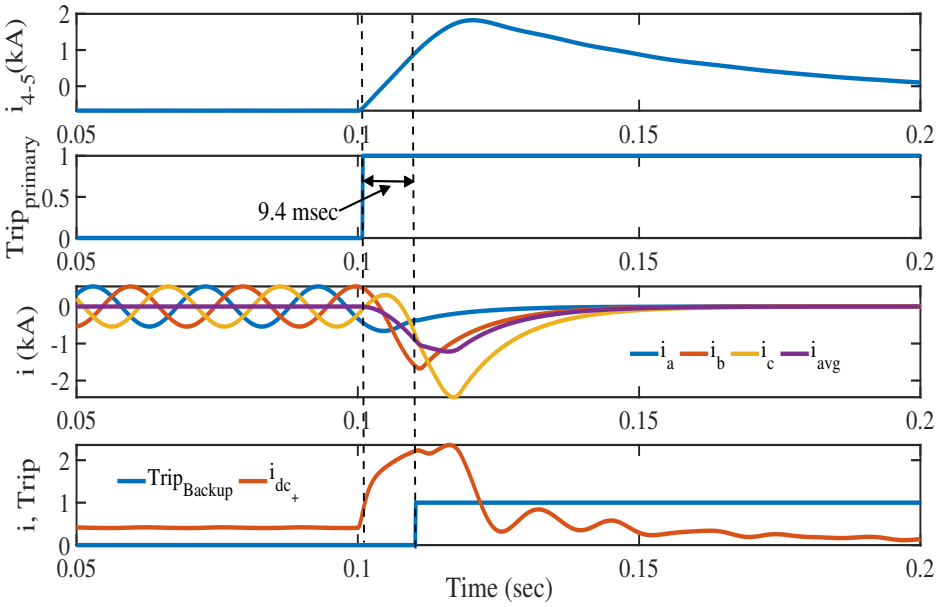

(a)

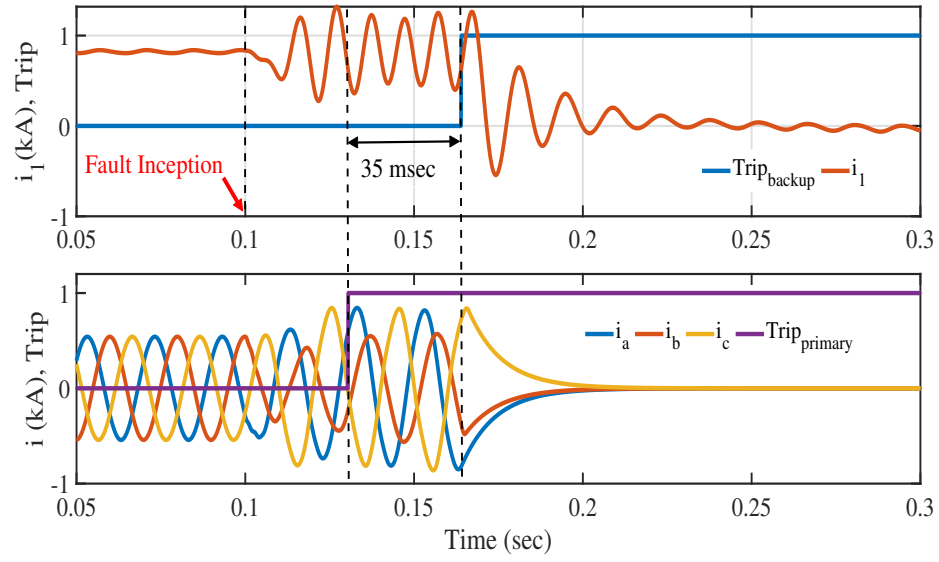

(b)

Figure 5.22: Protection coordination between primary and backup for (a) DC subgrid faults, (b) AC subgrid faults.

Table 5.4: Comparison with various Backup Protection Methods

Parameters/Features	**Various Methods**				
	Proposed	**[103]**	**[27]**	**[28]**	**[104]**
Microgrid Considered	Hybrid AC-DC	DC	AC	AC	DC
Signal required	Only I	Only I	Both, V and I	Both, V and I	Only V
Fault detection time	19 msec for DC subgrid fault and 46.3 msec for AC subgrid fault	1 msec	1.1 s	50 msec	1.015 msec
Sensitivity for high resistance fault	High	High	Low	Low	Low
HIL Validation	Yes	Yes	Low	No	Yes

detection time, sensitivity for high resistance faults, and available HIL validation. As shown in Table 5.4 the proposed scheme considered hybrid microgrid topology in contrast to other methods that considered either AC microgrid or DC microgrids. Proposed scheme require only AC and DC current at the BIC terminal to detect the fault on DC and AC subgrids, respectively. Whereas the methods in [27] and [28] require both voltage and current signals. Further, the HIL validation is made in the proposed scheme and the operating time is also compared with respect to simulation environment, in contrast to other methods given in Table 5.4.

5.9 Summary

In this work, a time-domain approach is proposed to provide backup protection for hybrid AC-DC microgrids. The proposed method isolates the faulty subgrid from the PCC. Analysis of AC and DC current at the terminal of BIC indicates the different characteristics during faults in AC and DC subgrids. The mode-0 and mode-1 currents at the BIC's DC terminal are obtained using symmetrical component decomposition. Consequently, the mode-1 current overlaid component is the primary discriminant between the AC and DC subgrid. Similarly, the one-cycle moving average and zero-crossing widths of the AC phase currents identify the faults in AC and DC subgrids. Hardware validation of the proposed method in real-time shows its strength. The proposed method works in the time domain and requires only a current sensor at both ends of the BIC. Therefore, it provides an economical and computationally efficient solution for the protection of hybrid AC-DC microgrids.